Journal of Hydroscience and Hydraulic Engineering
Vol. 18, No.1 May, 2000, 73-84

FDS AND FVM SCHEMES FOR 2-D FLOOD FLOW SIMULATIONS

By

Akhilesh Kumar Jha, Juichiro Akiyama and Masaru Ura

Department of Civil Engineering, Kyushu Institute of Technology
Tobata, Kitakyushu 804-8550, Japan.

SYNOPSIS

Numerical models based on flux-difference splitting (FDS) technique are developed for simulating rapidly varied flows in two-dimensional space co-ordinates. A first-order accurate model using Roe's numerical flux and a second-order accurate scheme using Lax-Wendroff numerical flux are constructed. Another model based on Finite Volume Method (FVM) is developed to examine validity of boundary approximation by finite-difference schemes. Roe's averaging for velocity and celerity ensures conservation and consistency while entropy satisfying solution is guaranteed by a theoretically sound treatment. Flux limiters used in the second-order accurate model yield oscillation-free results while maintaining high shock-resolution. The models' validity and applicability are demonstrated by comparing computed results with analytical and experimental results for 1D problems as well as with experimental results of 2D dam-break flows. Qualitative analysis and comparison for some other cases of 2D dam-break flows are also performed.

INTRODUCTION

It is often difficult to maintain conservation across a discontinuity and handle different features of signal propagation in sub- and supercritical flow regions with conventional models for two-dimensional flood propagation. The problem increases manifold in case of rapidly varied flows. Schemes such as MacCormack (1,2), although conservative, treat the problem in a lump-sum way and, therefore, cannot work well where such detail as direction of signal propagation becomes a dominant feature. On the other hand, schemes such as Gabutti (3), although correctly handle signal propagation, are non-conservative. It has been demonstrated in case of the Beam and Warming scheme(4), which handles signal propagation through flux-vector splitting, that significant enhancement in accuracy can be achieved by making the scheme fully conservative.

In comparison, several shock-capturing schemes based on Flux Difference Splitting (FDS) have been found to give very accurate results with rather ease (5,6). These schemes essentially apply upwind differencing to a linearized Riemann problem (7). While that takes care of directionality of signal propagation, the approximate Jacobian developed by Roe(7) enables conservative splitting of flux differences. The second-order accurate versions of this class of schemes suitably limit contribution of higher-order terms for oscillation-free results(8). Although the rigorous theoretical development for FDS schemes has been confined to 1D flows, their logical extensions for solving 2D problems recently appearing in the literatures(9,10,11) show significant promise for further development. The reported 2D models utilizing approximate Riemann solvers mostly use finite-volume methods (FVM) and rely on MUSCL technique for higher order of accuracy.

This paper follows FDS technique for developing 2D models. Both first- and second-order

accurate schemes on the basis of Roe and Lax-Wendroff numerical fluxes, respectively, are presented and their relative merits in simulating rapidly varied 2D flows are examined. An FVM model is developed to simulate 2D dam-break flood wave in a channel with curved boundaries and the result is compared with those obtained by finite-difference models using boundary approximation. Roe's (7) conservative and consistent averaging for velocity and celerity is supported by Harten and Hymen's(12) treatment that avoids unphysical solutions. The enhanced shock-resolution by the second-order scheme is kept free from any dispersion error by limiting the second-order flux through suitable flux limiters. The validity and applicability of the models are demonstrated by comparing numerical results with experimental and analytical solutions. Results for some test problems are also compared with previously reported solutions by other schemes.

GOVERNING EQUATIONS

The governing equations for two-dimensional free-surface flows can be written as

$$\frac{\partial \mathbf{U}}{\partial t}+\frac{\partial \mathbf{E}}{\partial x}+\frac{\partial \mathbf{F}}{\partial y}+\mathbf{S}=0 \tag{1}$$

where **U** is the vector of unknowns, **E** and **F** are components of flux vectors and **S** is the vector containing source and sink terms. These vectors are given by

$$\mathbf{U}=\begin{pmatrix} h & uh & vh \end{pmatrix}^T \tag{2a}$$

$$\mathbf{E}=\begin{pmatrix} uh & u^2h+0.5gh^2 & uvh \end{pmatrix}^T \tag{2b}$$

$$\mathbf{F}=\begin{pmatrix} vh & uvh & v^2h+0.5gh^2 \end{pmatrix}^T \tag{2c}$$

$$\mathbf{S}=\begin{pmatrix} 0 & -gh(S_{ox}-S_{fx}) & -gh(S_{oy}-S_{fy}) \end{pmatrix}^T \tag{2d}$$

where h = flow depth, u,v = flow velocity along x- and y-directions, respectively, g = acceleration due to gravity, S_o and S_f are bed and energy slopes, respectively. Once the technique for solving homogeneous part of Eq.(1) is established, the source term **S** can be incorporated separately without affecting the overall formulation. Therefore, the source term is dropped from the following considerations for the development of numerical technique.

In order to effectively and justifiably apply the Riemann solver and flux difference splitting technique developed for 1D problem to the 2D problem defined by Eq.(1), help is sought from the operator splitting technique(13). In effect, it means that instead of solving Eq.(1), we solve the following two equations successively.

$$\frac{\partial \mathbf{U}}{\partial t}+\frac{\partial \mathbf{E}}{\partial x}=0 \tag{3a}$$

$$\frac{\partial \mathbf{U}}{\partial t}+\frac{\partial \mathbf{F}}{\partial y}=0 \tag{3b}$$

These equations can now be viewed as a representation of the two-dimensional problem by a pair of one-dimensional problems. Therefore, the techniques developed for 1D problems can be directly applied to the above pair of equations. The equivalence of Eq.(1) and (3) is approximate, not exact. The solution of Eq.(3a) is described in the following and Eq.(4) can be solved in a similar way. The flux vector **E** is related to **U** through it's Jacobian **A** as

$$\mathbf{A}=\frac{\partial \mathbf{E}}{\partial \mathbf{U}}=\begin{pmatrix} 0 & 1 & 0 \\ c^2-u^2 & 2u & 0 \\ -uv & v & u \end{pmatrix} \tag{4}$$

where c is celerity defined as $c=(gh)^{1/2}$. The hyperbolic nature of the governing equations means that the Jacobian **A** has a complete set of independent and real eigenvectors expressed as

$$\begin{pmatrix} \mathbf{e}^1 & \mathbf{e}^2 & \mathbf{e}^3 \end{pmatrix}=\begin{pmatrix} 1 & 0 & 1 \\ u+c & 0 & u-c \\ v & c & v \end{pmatrix} \tag{5}$$

The corresponding eigenvalues are

$$\lambda^1=u+c;\quad \lambda^2=u\ ;\quad \lambda^3=u-c \tag{6a,b,c}$$

Roe(7) constructed an approximate Jacobian by using average values for velocity and celerity. The details of these averages in case of 1D shallow water equations may be referred to Jha et al.(5). Following similar arguments, the average velocities and celerity for a 2D problem can be obtained as

$$\tilde{u}=\left(u_R\sqrt{h_R}+u_L\sqrt{h_L}\right)\Big/\left(h_R+h_L\right) \tag{7a}$$
$$\tilde{v}=\left(v_R\sqrt{h_R}+v_L\sqrt{h_L}\right)\Big/\left(h_R+h_L\right) \tag{7b}$$
$$\tilde{c}=\sqrt{0.5g(h_R+h_L)} \tag{7c}$$

wherein the subscripts R and L refer to the right and left states (i.e. for i+1/2,j the left state is i,j and the right state is i+1,j).

FIRST-ORDER SCHEME

The first-order scheme for Eq.(3a) can be written as

$$\mathbf{U}_{i,j}^{t+1}=\mathbf{U}_{i,j}^{t}-\gamma\ \Delta\mathbf{E}_{i,j}^{t} \tag{8}$$

where i,j = space indices along x- and y-directions; t = time index; $\gamma=\Delta t/\Delta x$; Δt, Δx = time and space increments, respectively. The flux difference $\Delta\mathbf{E}$ is written in split form as

$$\Delta\mathbf{E}=\sum_{k=1}^{3}\alpha^k\left(\lambda^+ + \lambda^-\right)^k\mathbf{e}^k \tag{9}$$

where k = wave number and α = wave strength, expressed as

$$\alpha^1=0.5\Delta h+0.5\left(\Delta(uh)-\tilde{u}\,\Delta h\right)/\tilde{c} \tag{10}$$
$$\alpha^2=\left(\Delta(vh)-\tilde{v}\,\Delta h\right)/\tilde{c} \tag{11}$$
$$\alpha^3=\Delta h-\alpha^1 \tag{12}$$

The splitting of flux-difference allows introduction of upwinding into the scheme. Insertion of

Eq.(9) into Eq.(8) and subsequent mathematical manipulation yield the following first-order upwind finite-difference scheme

$$\mathbf{U}_{i,j}^{t+1} = \mathbf{U}_{i,j}^{t} - \gamma\left(\mathbf{E}_{i+1/2,j}^{N} - \mathbf{E}_{i-1/2,j}^{N}\right) \tag{13}$$

where the numerical flux $\mathbf{E}^N$ is expressed as

$$\mathbf{E}^N = 0.5\left(\mathbf{E}_R + \mathbf{E}_L\right) - 0.5\sum_{k=1}^{3} \tilde{\alpha}^k \left|\tilde{\lambda}^k\right| \tilde{\mathbf{e}}^k \tag{14}$$

The average velocities and celerity given by Eq.(7) are conservative and consistent with the governing equation. However, it converges to an unphysical solution by violating entropy inequality condition in case of rarefaction waves (dam-break case, for example). The problem can be overcome by replacing the modulus of λ in Eq.(14) by a small quantity δ whenever modulus of λ is less than δ (12). δ can be computed as (12).

$$\delta^k = \max\left(0, \lambda_{LR} - \lambda(\mathbf{U}_L), \lambda(\mathbf{U}_R) - \lambda_{LR}\right) \tag{15}$$

$$\lambda_{LR} = \lambda\left(\mathbf{U}_L, \mathbf{U}_R\right) \tag{16}$$

SECOND-ORDER SCHEME

The second-order accurate scheme is obtained by using Lax-Wendroff numerical flux in Eq.(13). Using the approximate Jacobian of Roe(7), the Lax-Wendroff numerical flux can be written as

$$\mathbf{E}^{N(LW)} = 0.5\left(\mathbf{E}_R + \mathbf{E}_L\right) - 0.5\sum_{k=1}^{3} \tilde{\alpha}^k \left|\tilde{\lambda}^k\right| \tilde{\mathbf{e}}^k + 0.5\sum_{k=1}^{3} \phi\, \tilde{\alpha}^k \left|\tilde{\lambda}^k\right| \left(1 - \gamma\left|\tilde{\lambda}^k\right|\right) \tilde{\mathbf{e}}^k \tag{17}$$

where ϕ is the flux limiter, designed to prevent oscillations due to second order of accuracy. The flux limiter is a non-linear function of

$$r_{i+1/2,j}^k = \left(\alpha_{i+1/2-\mathrm{sign}(\tilde{\lambda}_{i+1/2,j}^k),j}^k \Big/ \alpha_{i+1/2,j}^k\right) \tag{18}$$

We use Van Albada limiter (8) which is expressed as

$$\phi = (r + r^2)/(1 + r^2) \tag{19}$$

Eqs.(15) and (16) are implemented for satisfying entropy inequality condition just as in the case of first-order scheme.

NUMERICAL STABILITY

The schemes presented herein are explicit and, therefore, require strict observance of stability criteria for successful execution. The following criteria for the time step has been found to give stable results.

$$\Delta t \le C_n \frac{\min(\Delta x, \Delta y)}{\max(c + \sqrt{u^2 + v^2})} \qquad (20)$$

where C_n=the Courant number.

NUMERICAL RESULTS

The models are first verified against the Stoker solution(14) of 1D dam-break problem. The dam-break problem is considered in a (200m x 200m) domain which is horizontal and frictionless (Fig.1). The area is divided into 5m x 5m, cells 40 along each direction. The dam is placed parallel to y-direction at 100m from either end of the flood that separates reservoir and flood-plain. The initial water depths in reservoir, h_r and flood-plain, h_f are 10m and 5m, respectively. The whole dam is taken off at the initiation of computation that simulates total collapse of the dam, for which 1D analytical solution is applicable. The computed results at time 7+Δt seconds are compared against analytical solution in Fig.2. Both first and second-order models are found to compare excellently with the Stoker solution. The negative wave as well as the positive wave front are correctly captured by the models and, as expected, the higher-order of accuracy yields slightly better shock- resolution. It can also be Seen that there is no trace of any entropy violation due to the remedial treatment.

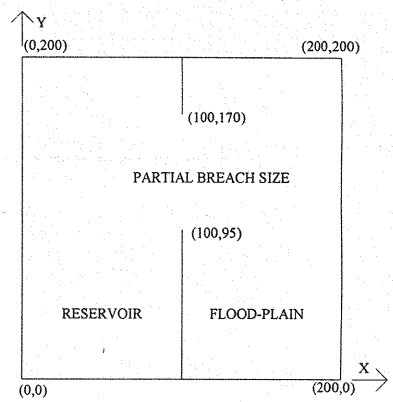

Fig.1 Definition sketch for dam-break problem.

The models are next verified against experimental data of a hydraulic jump from experiments conducted by Gharangik (15) in a 13.9m long and 0.45 m wide straight, horizontal, rectangular channel. The Manning's n for experimental conditions was reported between 0.008 and 0.011. The constant discharge was 0.053 m^3/s. The upstream flow depth was 0.064m (velocity=1.82m/s, F_r=2.3)

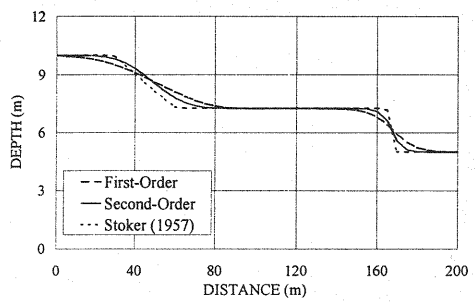

Fig.2 Comparison with analytical solution for the case of total dam collapse.

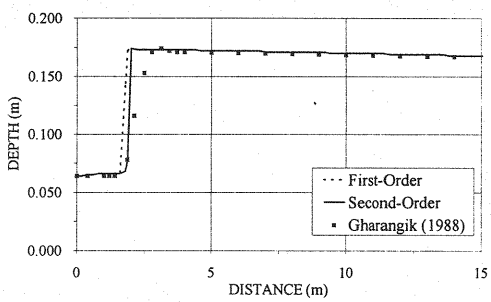

Fig.3 Hydraulic jump in rectangular channel.

and the conjugate depth was 0.17m (velocity=0.69m/s, Fr=0.53). The grid size for this problem is 0.05m x 0.05m. At the upstream end, both depth and velocity are specified and at the downstream end, a hypothetical rating curve is specified with a point corresponding to measured downstream conditions. We obtained good results with Manning's value equal to 0.008, which is well within reported values. The steady state results are compared with experimental data in Fig.3. The location of jump at about 1.6 m agrees well with the experimental data and so does the jump height. It may be noted, however, that the computed discontinuity is not as diffused as the observed one. This is due to the limitations of shallow water equations in computing diffusions within the jump.

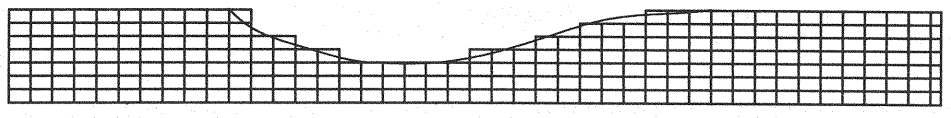

Fig. 4 Curved boundary of the computational domain approximated by rectangular mesh.

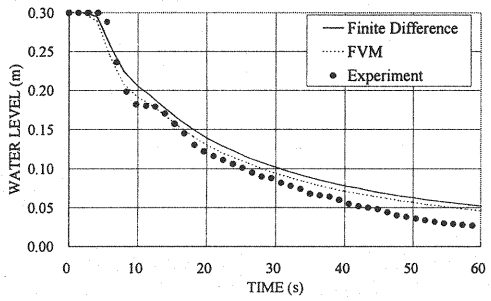

Fig.5 Depth hydrographs at x = 0.0 m
reservoir depth = 0.30m.

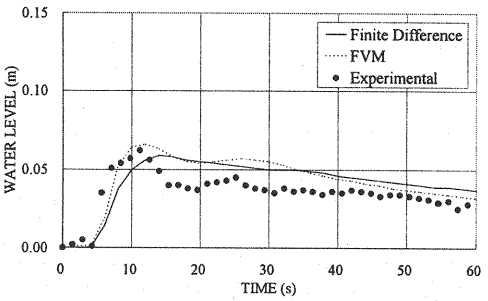

Fig.6 Depth hydrographs at x = 18.5 m
reservoir depth = 0.30m.

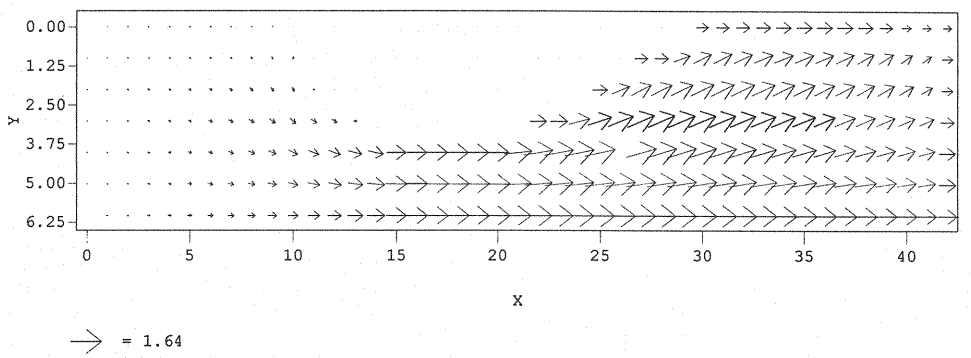

Fig.7 Velocity vector plot by finite difference model at 8s (Initial reservoir depth = 0.30m).

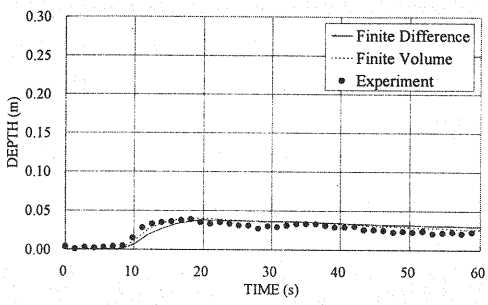

Fig.8 Depth hydrographs at x = 0.0 m reservoir depth = 0.15m.

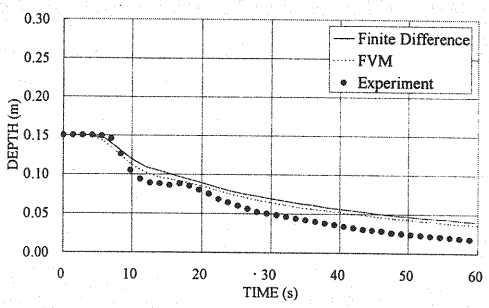

Fig.9 Depth hydrographs at x = 18.5 m reservoir depth = 0.15m.

Having verified the models with 1D problems, model's performance in case of 2D problems is examined with 2D dam-break problems. The first problem of 2D dam-break wave in flume is as described in Bellos et al.(16). The channel of variable slope is 21.2m long and 1.4m wide. Manning's coefficient for the flume material is specified as 0.012. The dam is placed at 8.5m from the upstream end. The measured water levels are available at 0.0m, 4.5m, 8.5m, 11.0m, 13.5m, 16.0m and 18.5m, measured from the upstream end. The flume width approaching the dam-section is gradually reduced while that downstream of the dam is gradually expanded. This converging-diverging geometry gives rise to 2D flow, most significantly in the converging-diverging region itself. Other details of the experimental set-up may be referred to Bellos et al. (16).

The computational domain is divided into rectangular meshes, 0.5m long (Δx) and 0.2m wide (Δy), giving 43 columns and 7 rows. It may be noted that the gradually curving boundary for the expansion and contraction, upstream and downstream of the dam, has been approximated by a series of rectangular meshes as shown in Fig.4. In order to see how this boundary approximation affects the results, a model based on Finite Volume Method (FVM) using Roe's (7) numerical flux has been developed. The details of the model are given in the appendix.

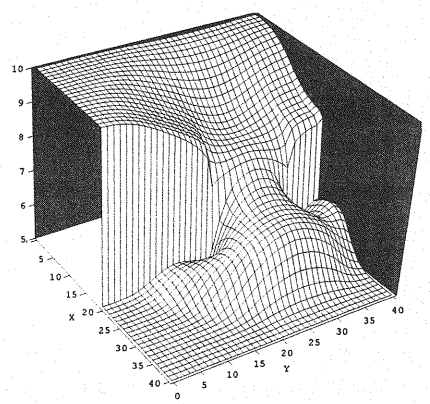

Fig.10 Water surface profile 7 sec. after partial dam-break. Computed by First-Order scheme (h_r/h_l=10/5).

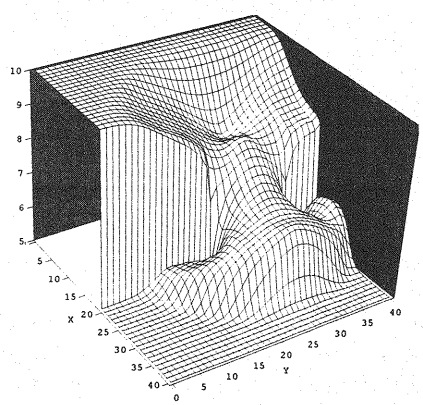

Fig.11 Water surface profile 7 sec. after partial dam-break. Computed by Second-Order scheme (h_r/h_l=10/5).

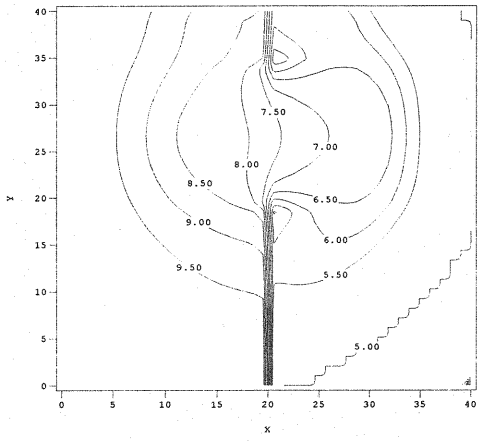

Fig.12 Water depth contour 7 sec. after partial dam-break by First-Order scheme (for Fig.10).

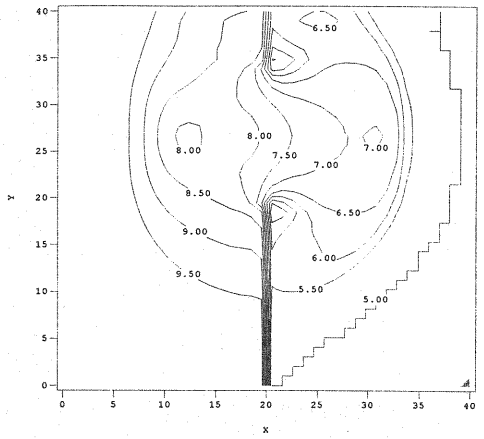

Fig.13 Water depth contour 7 sec. after partial dam-break by Second-Order scheme (for Fig.11).

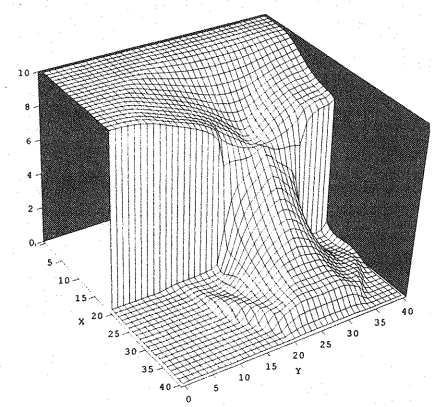

Fig.14 Water surface profile 7 sec. after partial dam-break computed by Second-Order scheme (h_r/h_f=10/.05).

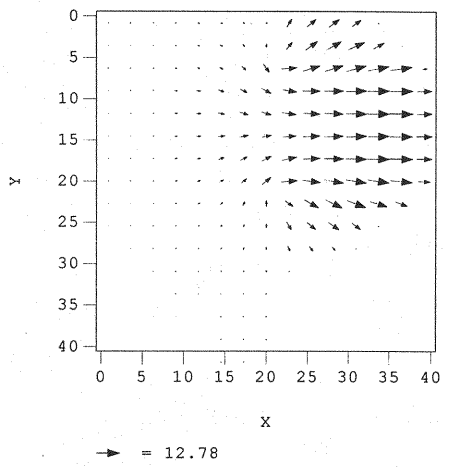

Fig.15 Velocity vectors corresponding Fig.14.

The results obtained by the second-order accurate model are presented for the case of horizontal flume bed. The initial condition downstream of the dam is dry floodplain. The initial conditions upstream of the dam, for the two cases simulated herein, are 0.30m and 0.15m deep still water. The computed depth hydrographs at upstream end of the flume and at 18.5m from the upstream end are shown in Figs.5 and 6 along with the experimental data. The results obtained by the FVM model, described in the appendix, are also given in Figs.5 and 6. It is seen from the figures that the computations reasonably reproduce experimentally recorded depths. There is no significant change in the results obtained by finite-difference and FVM models, indicating that boundary approximation in case of finite-difference model does not affect accuracy of the results.

Fig.7 shows velocity vector plot for this case as computed by the finite-difference model. The

approximation of a smoothly curved boundary by a series of rectangular meshes, as shown in Fig.4, does not seem to distort the velocity profile along the boundary.

Figs.8 and 9 show depth hydrographs at upstream end of the flume and at 18.5m from the upstream end in case of initial reservoir depth of 0.15m. The figures again include results by FVM model. The trend on accuracy of results, relative accuracy of finite-difference and FVM models as well as boundary approximation observed in case of Figs.5-7 are again confirmed by Figs.8 and 9.

The next example is taken from Fennema (17), for which results computed by other approaches have been previously reported(9,11,14). The problem is schematically shown in Fig.1 with the partial breach section. The simulated results are shown in Figs.10 and 11. The first-order model yields remarkably good results but the shock–resolution is less sharp than that given by the second-order accurate scheme.

The flow depth contours corresponding to Figs.10 and 11 are shown in Figs.12 and 13. These results look reasonable and compare very well with previously reported results(9,11,14).

In order to demonstrate the models' capability to simulate one of the severest problems, the water depth, h_t in the flood-plain is reduced to 0.05m. The water surface profile at $7+\Delta t$ seconds computed by second-order scheme is shown in Fig.14. The figure indicates that the bore travels much faster than when the flood-plain had larger water depth. However, the bore height is lower and less pronounced in this case. Fig.15 shows the corresponding velocity vector plot. It clearly shows that the velocity in the main flow direction is much larger than that in the transverse direction. Therefore, the flood-wave spreads comparatively slowly in the direction perpendicular to the main flow. Comparing Fig.15 with the velocity vector plot of Fig.16, corresponding to Fig.11, it is clear that this phenomenon becomes stronger as the difference between reservoir and floodplain depth increases.

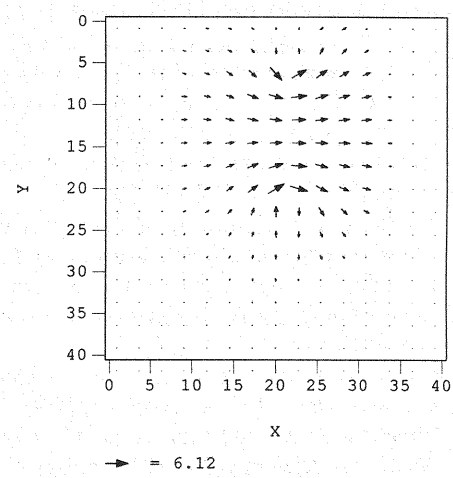

Fig.16 Velocity vectors for Fig.11.

It may be noted that a free-slip boundary condition has been implemented at side walls, which means that there is no side wall friction.

CONCLUSIONS

A First-order FDS scheme based on Roe's numerical flux and a second-order FDS scheme based on Lax-Wendroff numerical flux are developed for simulating rapidly varied two-dimensional flows. An FVM model is constructed to simulate curved boundaries and the results are compared against that obtained by finite-difference models through boundary approximation. These schemes incorporate Roe's approximate Jacobian for conservative properties and consistency with the governing equations. The inclusion of Harten and Hymens treatment ensures models' compliance with entropy inequality requirements. The models are applied to severe 1D dam-break and hydraulic jump problems. The models are verified against experimental and qualitative data of 2D dam-break flow. The comparison of numerical results with analytical and experimental results indicates that the models presented in this paper yield accurate results, both for 1D and 2D problems. It is also found through comparison with the FVM model that the proposed finite-difference models yield accurate results even in case of boundaries that are not aligned with the rectangular grid system. No

significant difference is noticed in the results by the FDS and FVM models. The shocks are resolved, particularly by the second-order scheme, mostly within one spatial grid. The mass balance was tracked in all cases and the error was always within one percent. It is concluded that these models can be used confidently to simulate 2D rapidly varied flows.

REFERENCES

1. Bhallamudi, S. M. and Chaudhry, M. H.: Computation of flows in open-channel transition., *J. of Hyd. Res.*, Vol.30, No.1, pp.77-93, 1992.
2. Rahman, M. and Chaudhry, M. H.: Computation of flow in open-channel transition, *J. of Hyd. Res.*, Vol.35, No.2, pp.243-256, 1997.
3. Gabutti, B.: On two upwind finite-difference schemes for hyperbolic equations in non-conservation form, *Computer and Fluids*, Vol.11, No.3, pp.207-230, 1983.
4. Jha, A. K., Akiyama, J. and Ura, M.: A fully conservative Beam and Warming scheme for transient open channel flows, *J. of Hyd. Res.*, Vol.34, No.5, pp.605-621, 1996.
5. Jha, A. K., Akiyama, J. and Ura, M.: First- and second-order flux difference splitting schemes for dam-break problem, *J. of Hyd. Engineering, ASCE.*, Vol.121, No.12, pp.877-884, 1995.
6. Glaister, P.: Approximate Riemann solutions of the shallow water equations, *J. of Hyd. Res.*, Vol.26, No.3, pp.293-306, 1988.
7. Roe, P. L.: Approximate Riemann solvers, parameter vectors and difference schemes, *J. Comp. Physics*, Vol.43, pp.357-372, 1981.
8. Sweby, P. K.: High resolution schemes using flux limiters for hyperbolic conservation laws., *SIAM J. Numer. Anal.*, Vol.21, pp.995-1101, 1984.
9. Alcrudo, F., Garcia-Navarro, P. and Saviron, J. M.: A high-resolution Godunov-type scheme in finite volumes for the 2D shallow water equations, *J. Numer. Methods in Fluids*, Vol.16, pp.489-505, 1993.
10. Glaister, P.: Approximate Riemann solutions of the two-dimensional shallow-water equations, *J. of Enggr. Math.*, Vol.24, pp.45-53, 1990.
11. Mingham, C. G. and Causon, D. M.: High-resolution finite-volume method for shallow water flows, *J. of Hyd. Res.*, Vol.124, No.6, pp.605-614, 1998.
12. Harten , A. and Hymen, J. M.: Self adjusting grid method for one-dimensional hyperbolic conservation laws, *J. Comp. Physics*, Vol.50, pp.235-269, 1983.
13. Yanenko, N. N.: The method of fractional steps, Springer-Verlag, Berlin, 1971.
14. Stoker, J. J. :Water Waves, Interscience Publishers Inc., Wiley and Sons, New York, 1957.
15. Gharangik, A. M.: Numerical simulation of hydraulic jump, M.Sc. thesis, Washington State University, Wash. U.S.A., 1988.
16. Bellos, C. V., Soulis, J. V. and Sakkas, J. G.: Experimental investigation of two-dimensional dam-break induced flows, J. Hyd. Res., Vol.30, No.1, pp.47-63, 1992.
17. Fennema, R. J.: Numerical simulation of two-dimensional transient free-surface flows, Ph. D. Dissertation, Washington State University, Pullman, U.S.A., 1985.

ACKNOWLWDGEMENTS

This research was supported by the Grant-in-Aid for Science Research for Ministry of Education and Culture, Japan under Grant B(2), No. 11450190.

APPENDIX – FVM Model

Here we briefly explain the FVM model developed to simulate some of the 2D dam-break flows, the results of which are shown in Figs.5,6,8 and 9. The homogeneous part of the governing equation, Eq.1 without the source term, can also be written as,

$$\frac{\partial \mathbf{U}}{\partial t} + \nabla \mathbf{G} = 0 \tag{A.1}$$

The integral form of the governing equation is obtained by integrating Eq.(A.1) over the area of a cell, A_0 as

$$\int_V \left(\frac{\partial \mathbf{U}}{\partial t} + \nabla \mathbf{G} \right) dV = \int_V \frac{\partial \mathbf{U}}{\partial t} dV + \oint_{A_0} (\mathbf{G}.\mathbf{n}) dA_0 = 0 \tag{A.2}$$

where $\mathbf{G}.\mathbf{n} = \mathbf{E}n_x + \mathbf{F}n_y$, n_x and n_y = components of normal vector n along x and y-directions, respectively. Eq.(A.2) can be simplified by assuming that the flow variables remain constant within a cell and that the surface integral can be evaluated as a sum of the numerical flux over the walls of a cell. Thus, the FVM model is obtained as

$$\mathbf{U}^{t+1} = \mathbf{U}^t - \frac{A_0}{\Delta t} \sum_{s=1}^{ns} \left(\mathbf{G}_s^*.\mathbf{n}_s \right) dl_s \tag{A.3}$$

The numerical flux $\mathbf{G}^*$ can be computed as in Eq.(14) and Roe's average variables are given as in Eq.(7). However, the eigenvectors are computed by

$$\left(\mathbf{e}^1 \quad \mathbf{e}^2 \quad \mathbf{e}^3 \right) = \begin{pmatrix} 1 & 0 & 1 \\ \tilde{u} + \tilde{c}n_x & -\tilde{c}n_y & \tilde{u} - \tilde{c}n_x \\ \tilde{v} + \tilde{c}n_y & \tilde{c}n_x & \tilde{v} - \tilde{c}n_y \end{pmatrix} \tag{A.4}$$

The corresponding eigenvalues are

$$\lambda^1 = \tilde{u}n_x + \tilde{v}n_y + \tilde{c}\,; \quad \lambda^2 = \tilde{u}n_x + \tilde{v}n_y \;; \quad \lambda^3 = \tilde{u}n_x + \tilde{v}n_y - \tilde{c} \tag{A.5}$$

The wave strengths are computed by

$$\alpha^1 = 0.5\Delta h + 0.5\left(\Delta(uh)n_x + \Delta(vh)n_y - \tilde{\mathbf{u}}.\mathbf{n}\,\Delta h \right)/\tilde{c} \tag{A.6}$$

$$\alpha^2 = \left[\left(\Delta(vh) - \tilde{v}\,\Delta h \right)n_x - \left(\Delta(uh) - \tilde{u}\,\Delta h \right)n_y \right]/\tilde{c} \tag{A.7}$$

$$\alpha^3 = \Delta h - \alpha^1 \tag{A.8}$$

This complets description of the FVM model used in this paper.

APPENDIX - NOTATION

The following symbols are used in this paper :

$\mathbf{A}$ = Jacobina of $\mathbf{E}$;
A_0 = Area of a cell;
C_n = Courant number;
$\mathbf{E}$ = flux matrix on fixed grid;
$\mathbf{E}^N$ = numerical flux;
$\mathbf{F}$ = numerical flux on fixed grid;
K = wave number;
$\mathbf{S}$ = matrix containing source terms;
S_f = friction slope;
S_o = bed slope
$\mathbf{U}$ = vector for flow variables;
c = celerity;
$\mathbf{e}$ = matrix of eigenvectors of $\mathbf{A}$;
g = acceleration due to gravity;
h = flow depth;
r = ratio of wave strength for flux limiter;
u = velocity in x-direction;
v = velocity in y-direction;
Δt = Time step;
Δx = grid size in x-direction;
α = wave strength;
δ = small positive quantity;
ϕ = flux limiter;
γ = $\Delta t/\Delta x$; and
λ = eigenvalues of $\mathbf{A}$.

(Received December 9, 1999 ; revised February 22, 2000)